OPEN

Citation: Cell Death and Disease (2013) 4, e911; doi:10.1038/cddis.2013.445

www.nature.com/cddis

Insulin-like growth factor binding proteins 4 and 7 released by senescent cells promote premature senescence in mesenchymal stem cells

V Severino[1,2,3,10], N Alessio[4,10], A Farina[5], A Sandomenico[2,3], M Cipollaro[4], G Peluso[6,7], U Galderisi*[,4,6,8,9] and A Chambery*[,1,3]

Cellular senescence is the permanent arrest of cell cycle, physiologically related to aging and aging-associated diseases. Senescence is also recognized as a mechanism for limiting the regenerative potential of stem cells and to protect cells from cancer development. The senescence program is realized through autocrine/paracrine pathways based on the activation of a peculiar senescence-associated secretory phenotype (SASP). We show here that conditioned media (CM) of senescent mesenchymal stem cells (MSCs) contain a set of secreted factors that are able to induce a full senescence response in young cells. To delineate a hallmark of stem cells SASP, we have characterized the factors secreted by senescent MSC identifying insulin-like growth factor binding proteins 4 and 7 (IGFBP4 and IGFBP7) as key components needed for triggering senescence in young MSC. The pro-senescent effects of IGFBP4 and IGFBP7 are reversed by single or simultaneous immunodepletion of either proteins from senescent-CM. The blocking of IGFBP4/7 also reduces apoptosis and promotes cell growth, suggesting that they may have a pleiotropic effect on MSC biology. Furthermore, the simultaneous addition of rIGFBP4/7 increased senescence and induced apoptosis in young MSC. Collectively, these results suggest the occurrence of novel-secreted factors regulating MSC cellular senescence of potential importance for regenerative medicine and cancer therapy.
Cell Death and Disease (2013) **4,** e911; doi:10.1038/cddis.2013.445; published online 7 November 2013
Subject Category: Experimental Medicine

Senescence is the permanent cell cycle arrest that leads to the loss of cellular functions over time. Several lines of evidence correlate cellular senescence to aging, as it largely contributes to reduce tissue functions and renewal. On the other side, it is also believed to promote protective anticancer mechanisms leading to tumor growth arrest.[1,2]

Senescence of stem cells, such as mesenchymal stem cells (MSCs), could be very deleterious as it can greatly impair tissue homeostasis and repair. MSC are pluripotent cells that reside in postnatal organs and tissues, and can differentiate into bone, cartilage and fat. Owing to their supporting role in hematopoiesis and in the homeostatic maintenance of many organs and tissues, MSC also have a significant therapeutic potential for tissue regeneration.[3–5]

Cellular senescence has been for long time considered as an exquisitely intracellular event unleashed by activation of a cytoplasmic signaling circuitry. Recent studies have evidenced that a pool of molecules secreted by senescent cells, for which the term 'senescence-associated secretory phenotype' (SASP) has been proposed, is associated and may contribute to cellular proliferative arrest through autocrine/paracrine pathways.[6–8] Secreted factors can regulate the senescence response and may represent a danger signal that sensitizes normal neighboring cells to senesce, thus enhancing the ability of damaged cells to enter senescence. In advanced tumor phases, however, cancer cells can take advantage of signaling pathways induced by secreted factors for their growth.[6]

MSC's beneficial influence in tissue repair has also been attributed to their paracrine activity.[9,10] Therefore, changing the pattern of factors secreted by MSC during the senescence process may have a great impact on body's health. Given the

[1]Department of Environmental, Biological and Pharmaceutical Sciences and Technologies, Second University of Naples, Caserta, Italy; [2]Institute of Biostructures and Bioimaging-IBB, CNR, Napoli, Italy; [3]Centro Interuniversitario di Ricerca sui Peptidi Bioattivi-CIRPEB, Napoli, Italy; [4]Department of Experimental Medicine, Biotechnology and Molecular Biology Section, Second University of Naples, Napoli, Italy; [5]Biomedical Proteomics Research Group, Department of Bioinformatics and Structural Biology, Geneva University, Geneva, Switzerland; [6]Institute of Protein Biochemistry and Bioresources-IBP, CNR, Napoli, Italy; [7]Institute of Biosciences and Bioresources-IBBR, CNR, Napoli, Italy; [8]Sbarro Institute for Cancer Research and Molecular Medicine, Center for Biotechnology, Temple University, Philadelphia, PA, USA and [9]Genome and Stem Cell Center-GENKOK, Erciyes University, Kayseri, Turkey
*Corresponding authors: A Chambery, Department of Environmental, Biological and Pharmaceutical Sciences and Technologies, Second University of Naples, Caserta I-81100, Italy. Tel: +39 0823 274535; Fax: +39 0823 274571; E-mail: angela.chambery@unina2.it
or U Galderisi, Department of Experimental Medicine, Biotechnology and Molecular Biology Section, Second University of Naples, Napoli I-80138, Italy. Tel: +39 081 5667585; Fax: +39 081 5667547; E-mail: umberto.galderisi@unina2.it
[10]These authors contributed equally to this work.
Keywords: senescence; mesenchymal stem cells; IGFBP4; IGFBP7; mass spectrometry; secretome
Abbreviations: CM, conditioned medium; ECM, extracellular matrix; ERK, extracellular signal-regulated kinases; IGF, insulin growth factor; IGFBP4, insulin-like growth factor binding proteins 4; IGFBP7, insulin-like growth factor binding proteins 7; LC-MS, liquid chromatography-mass spectrometry; MSC, mesenchymal stem cells; MUG, 4-methylumbelliferyl-β-D-galactopyranoside; SA-β-gal, senescence-associated β-galactosidase; SASP, senescence-associated secretory phenotype; SMS, senescence-messaging secretome
Received 11.6.13; revised 31.7.13; accepted 12.9.13; Edited by Y SHi

paramount importance of autocrine/paracrine signaling in MSC functions, elucidating the composition of the pool of proteins secreted by MSC would enhance our understanding on how these cells affect the environment niche, and support tissue repair, immunomodulation, hematopoietic stem cell self-renew, and tumor growth. To date, studies on the MSC secretome are still in their infancy and mainly refer to the high potential of MSC secretome for the development of therapeutic strategies for the treatment of diseases.[11,12]

To our knowledge, a comprehensive analysis of the secretome profile of senescent MSC is lacking. In this work, the senescence-inducing properties of conditioned medium (CM) of senescent MSC have been investigated. A 'bottom-up' proteomics approach based on liquid chromatography-mass spectrometry (LC-MS/MS) label-free quantitative analysis has been used to identify and compare the expression levels of secreted proteins in the MSC CM at early and late cultivation phases. Our results provide a detailed characterization of the MSC secretome associated to the senescent phenotype, revealing that selected components of the insulin-like growth factor binding proteins (IGFBPs) family are strongly involved in MSC SASP. We have identified IGFBP4 and IGFBP7 as important senescence-inducing factors, as their single and/or simultaneous immunodepletion abolishes the pro-senescent effect of senescent MSC CM, reduces apoptosis and promotes cell growth. Moreover, the simultaneous addition of rIGFBP4/7 increased senescence and induced apoptosis in MSC. Predicting stem cell fate requires knowledge of how extracellular stimuli are integrated with intracellular signaling networks. Results from an *in silico* analysis suggest that the extracellular signal-regulated kinases (ERK 1/2) is one of the converging node of the MSC SASP. Accordingly, the induction of MSC senescence program impairs the nuclear/cytosolic localization of active ERK. This study provides an important basis for deciphering the complex extracellular protein networks implicated in MSC cellular senescence and their interplay with the corresponding cytoplasmic signaling circuitry.

Results

CM from senescent MSC triggers senescence in young cells. Senescence of stem cells is caused by a combination of intrinsic irreversible and reversible changes also influenced by circulating effectors or factors secreted by local stem cell niches.[13] Therefore, we decided to investigate the effects of extrinsic signaling on MSC senescence. At first, properties of young (passage 1, P1) and senescent (passage 10, P10) MSC were evaluated. Following senescence induction, MSC showed a characteristic phenotype including larger and flattened cell morphology (Figure 1a). As expected, proliferation rate was significantly lower in P10 *versus* P1 cultures (Figure 1b), and this decrease was associated with an increased percentage of senescent cells (Figure 1c). No significant changes in the apoptotic rate were detected (Figure 1c), confirming the presence of a higher percentage of senescent MSC in P10 compared with P1 cultures.

To determine whether extracellular factors were endowed with senescence-induction properties, proliferation rate, apoptosis and senescence were evaluated on young MSC cultured with CM from senescent cells (CM-P10). A complementary experiment was performed by culturing senescent cells with CM-P1 from young MSC (Figure 1d). Results demonstrate that CM-P10 was able to trigger senescence in young MSC as suggested by a significant reduction in their proliferation rate (Figure 1e) and confirmed by 4-methylumbelliferyl-β-D-galactopyranoside (MUG) and senescence-associated β-galactosidase (SA-β-gal) assays (Figures 1g, h–j). No modification of the apoptotic rate was detected (Figures 1i–k). The specificity of the observed senescence response was attested by the evidence that the incubation of P10 MSC cultures with CM-P1 did not induce any significant change in proliferation, senescence and apoptosis (Figures 1f–k). These results demonstrate that extrinsic factors secreted by senescent MSC are able to promote senescence phenomena in neighboring cells. Once triggered, the senescence process appears to be irreversible, or at least it cannot be reverted by secreted factors produced by young MSC.

Secretome analysis of MSC CM. To identify candidate proteins responsible for the senescence-inducing properties of CM-P10 and to delineate a hallmark of MSC senescent phenotype, a comparative secretome analysis was performed by applying a shotgun proteomics strategy. CM-P1 and CM-P10 were processed for protein precipitation by trichloroacetic acid, and LC-ESI-MS/MS analyses were carried out on peptides deriving from tryptic digestion of proteins. Using high-resolution MS and Mascot database search, 121 proteins were qualitatively identified across both conditions in the MSC secretome. Data were filtered on the basis of probability of protein identification and technical reproducibility, allowing the selection of 66 non-redundant proteins (Supplementary Information, Supplementary Tables S1 and S2). The quantitative analysis performed by spectral counting revealed that 33 proteins were common to both CM-P1 and CM-P10 with no significant differences in their expression levels (Supplementary Information, Supplementary Table S3). Among differentially expressed proteins, 7 and 13 proteins were uniquely detected in CM-P1 and CM-P10, respectively (Table 1a), whereas a set of proteins was significantly up- and downregulated in CM-P10 *versus* CM-P1 (Table 1b).

The identified proteins were analyzed for classical (i.e., signal peptide-driven secretion through the ER/Golgi pathway[14]) and non-classical (e.g., proteins released through vesicles and extracellular matrix (ECM) proteins[15]) secretion pathways, revealing that about 94% of the identified proteins were predicted to be secreted. Among them, 57 proteins ($\sim$93%) were endowed with the signal peptide for secretion through the ER/Golgi pathway, whereas only four additional proteins ($\sim$7%) were predicted to be released by cells through non-classical secretion mechanisms.

A bioinformatic analysis performed by using the Metacore software revealed that a significant number of differentially regulated proteins was involved in cell–matrix interactions, ECM regulation and protein-folding response (Figure 2a). In detail, the heat map distribution of these proteins show that several upregulated proteins in senescent MSC were involved in cell adhesion, ECM remodeling and connective tissue

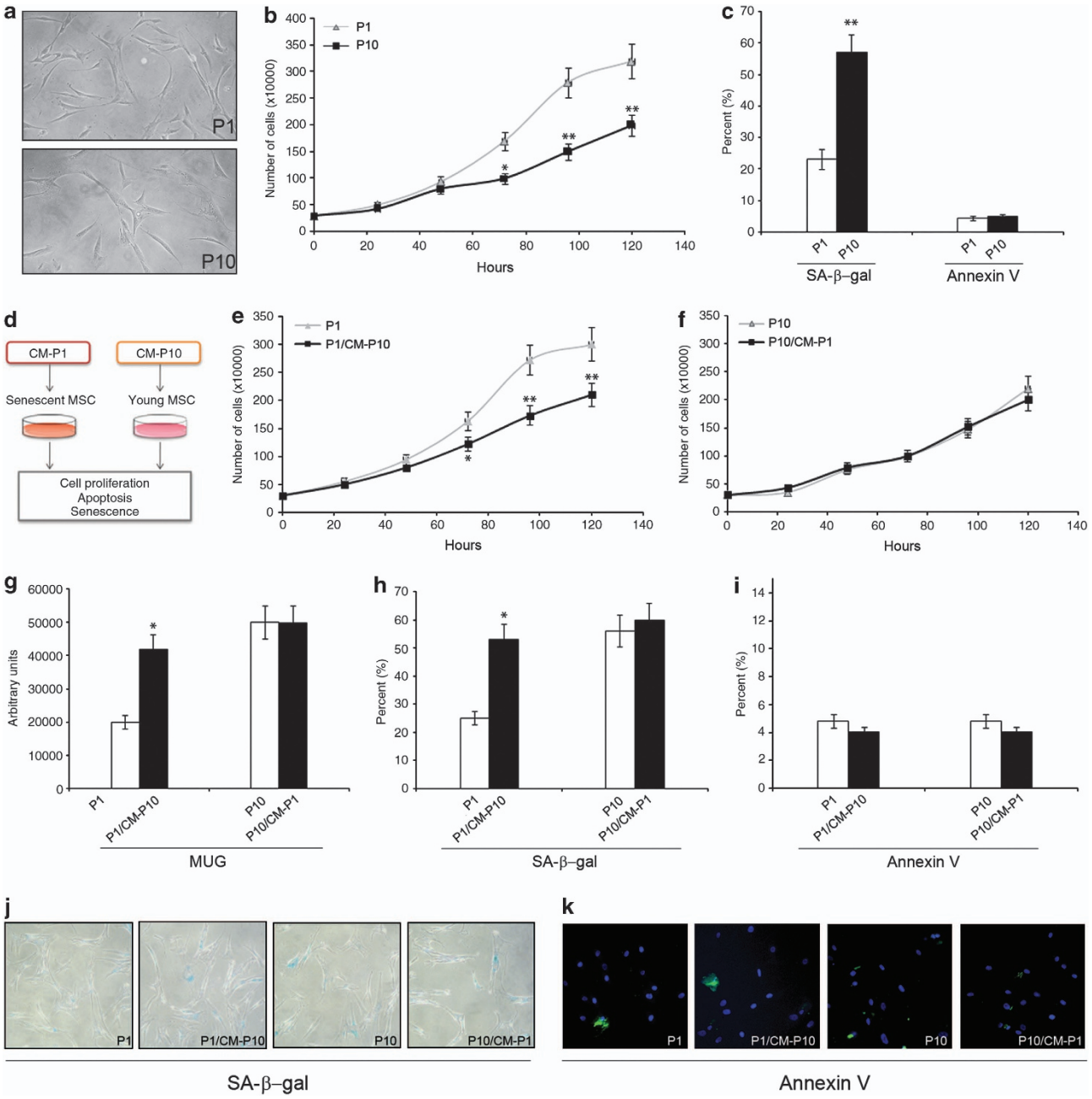

Figure 1 CM from senescent MSC triggers senescence in young cells. (**a**) Induction of replicative senescence was accomplished by repeatedly passaging the cells at P10. Following senescence induction, MSC showed a characteristic phenotype including larger and flattened cell morphology with respect to young MSC (P1). (**b**) Cell proliferation measured by Quick Cell Proliferation Colorimetric Assay Kit II. $^{*}P<0.05$; $^{**}P<0.01$ *versus* P1. (**c**) Percentage of SA-β-gal-positive cells; $^{**}P<0.01$ *versus* P1. Apoptotic cells were detected using fluorescein-conjugated Annexin V staining on P1 and P10 MSC. (**d**) Schematic summary of the experimental workflow for the evaluation of the effects of MSC CM on cell proliferation, apoptosis and senescence. (**e**) Cell proliferation rate evaluated on young MSC cultured with CM-P10 (P1/CM-P10); $^{*}P<0.05$; $^{**}P<0.01$ *versus* P1 MSC grown in control medium. (**f**) Cell proliferation rate evaluated on senescent MSC cultured with CM-P1 (P10/CM-P1). (**g–i**) MUG, SA-β-gal and Annexin V assays performed on P1/CM-P10 and on P10/CM-P1; $^{*}P<0.05$ *versus* MSC grown in control medium. For all assays, values are means of three independent experiments. (**j**) Representative microscopic fields of SA-β-gal-positive cells (blue). The mean percentage value of senescent cells ($\pm$S.D., $n=3$) is reported in Figure 1h. (**k**) Micrographs showing merge of representative fields of P1 and P10 MSC grown under different conditions and stained with Annexin V (green) are showed. Nuclei were counterstained with Hoechst 33342 (blue). The mean percentage value of apoptotic cells ($\pm$S.D., $n=3$) is indicated in Figure 1i

degradation (Figure 2b). Several collagen components involved in cartilage development and integrin-mediated cell–matrix adhesion were also upregulated in senescent cells. Furthermore, proteins involved in ER-associated and cytoplasm protein-folding response were downregulated in senescent MSC (Figure 2b).

Key molecules of the IGF signaling pathway were also differentially regulated in senescent with respect to young

Table 1 Proteins uniquely (a) and differentially regulated (b) identified in CM-P1 and CM-P10 secretome by high-resolution LC-MS/MS

(a)

ID	Accession	Protein name	Mr (kDa)	No. of peptides	Secretome P^a	Signal P^b
CM-P1	P27797	Calreticulin	48	3	0.37	Y
	P27658	Collagen alpha-1(VIII) chain	73	2	0.38	Y
	O43854	EGF-like repeat and discoidin I-like domain-containing protein 3	54	2	0.82	Y
	P14625	Endoplasmin	92	2	0.50	Y
	P08238	Heat-shock protein HSP 90-beta	83	4	0.20	N
	P51884	Lumican	38	8	0.54	Y
	P23284	Peptidyl-prolyl cis-trans isomerase B	24	2	0.85	N
CM-P10	Q9BRK5	45 kDa calcium-binding protein	42	3	0.59	Y
	P16112	Aggrecan core protein	250	6	0.57	Y
	P49747	Cartilage oligomeric matrix protein	83	2	0.27	Y
	P01034	Cystatin-C	16	2	0.94	Y
	Q4ZHG4	Fibronectin type III domain-containing protein 1	206	2	0.14	Y
	P24593	Insulin-like growth factor binding protein 5	31	2	0.92	Y
	Q9Y287	Integral membrane protein 2B	30	2	0.84	N
	Q08397	Lysyl oxidase homolog 1	63	3	0.52	Y
	Q09666	Neuroblast differentiation-associated protein AHNAK	629	2	0.24	N
	P62937	Peptidyl-prolyl cis-trans isomerase A	18	3	0.34	N
	P10124	Serglycin	18	2	0.72	Y
	Q7Z7G0	Target of Nesh-SH3	119	2	0.21	Y
	P24821	Tenascin	241	2	0.47	Y

(b)

ID	Accession	Protein name	Mr (kDa)	No. of peptides	CM-P10/ CM-P1	*P*-value	Secretome P^a	Signal P^b
Down	P21810	Biglycan	42	6	0.45	0.022	0.71	Y
	P12109	Collagen alpha-1(VI) chain	109	11	0.58	0.003	0.23	Y
	P12110	Collagen alpha-2(VI) chain	109	6	0.23	0.001	0.21	Y
	P12111	Collagen alpha-3(VI) chain	344	10	0.53	0.006	0.32	Y
	P35555	Fibrillin-1	312	13	0.56	0.003	0.39	Y
	Q15063	Periostin	93	8	0.33	0.002	0.27	Y
Up	Q99715	Collagen alpha-1(XII) chain	333	52	1.98	0.023	0.33	Y
	P08123	Collagen alpha-2(I) chain	129	51	1.80	0.025	0.34	Y
	P08572	Collagen alpha-2(IV) chain	168	9	2.8	0.034	0.07	Y
	P21333	Filamin-A	281	15	7.75	1.4E-04	0.45	N
	P22692	Insulin-like growth factor binding protein 4	28	5	3.63	0.011	0.89	Y
	Q16270	Insulin-like growth factor binding protein 7	29	9	4.00	0.004	0.54	Y
	P08670	Vimentin	54	29	2.24	0.013	0.51	N

The Scaffold Software was used to improve protein identification by filtering data following the acceptance criteria of probability greater than 95.0%, as specified by the Protein-Prophet algorithm. The higher number of unique peptides for each protein identification is reported. Mr denotes relative molecular mass
[a]Secretion prediction according to Secretome P 2.0 server. Proteins with NN-score ≥ 0.5 are predicted as secreted by non-classical secretory pathways
[b]Secretion prediction according to signal peptide probability of Signal P 4.0 server. Y and N indicate the presence or absence of the signal peptide for secretion

MSC, including several IGFBPs, that are known to have a role in the induction of senescence and cancer.[6] In particular, a strong upregulation of IGFBP4 and IGFPB7 was observed in senescent cells, suggesting a role for these factors in triggering senescent phenomena in MSC.

IGFBP4 and IGFBP7 are key factors of senescent MSC CM for triggering senescence phenomena in young MSC. To determine the role of IGFBP4 and IGFBP7 in senescence, cell proliferation, apoptosis and senescence studies were undertaken on young MSC treated with IGFBP4- and/or IGFBP7-immunodepleted CM-P10 (Figure 3a). As, shown, treatment with anti-IGFBP4 and/or anti-IGFBP7 blocked the pro-senescence activity of CM-P10 even at the lowest concentration tested (Figure 3b). It is to be noted that the simultaneous treatment with both anti-IGFBP4 and anti-IGFBP7 provided an enhanced reduction of senescence induced by CM-P10 on P1 MSC (Figure 3b). Notably, the percentage of senescent cells in P1 cultures incubated with IGFBP4- and IGFBP7-immunodepleted CM-P10 was even lower than control. The analysis of the chromatin status is an additional crucial aspect for an in depth investigation of senescence phenomena. It has been shown that distinct heterochromatin structures accumulate during senescence and could represent a hallmark of this process.[16] In P1 cultures incubated with IGFBP4- and/or IGFBP7-immunodepleted CM-P10, a significant reduction of the HP1 alpha- and H3K9me3-positive cells compared with those supplemented with untreated CM-P10 was observed (Figures 3c–f and Supplementary Information, Supplementary Figure S1). This effect was further enhanced by the simultaneous use of both IGFBP4 and IGFBP7 antibodies. In addition, treatment of CM-P10 with both anti-IGFBP4 and anti-IGFBP7 showed a significant reduction

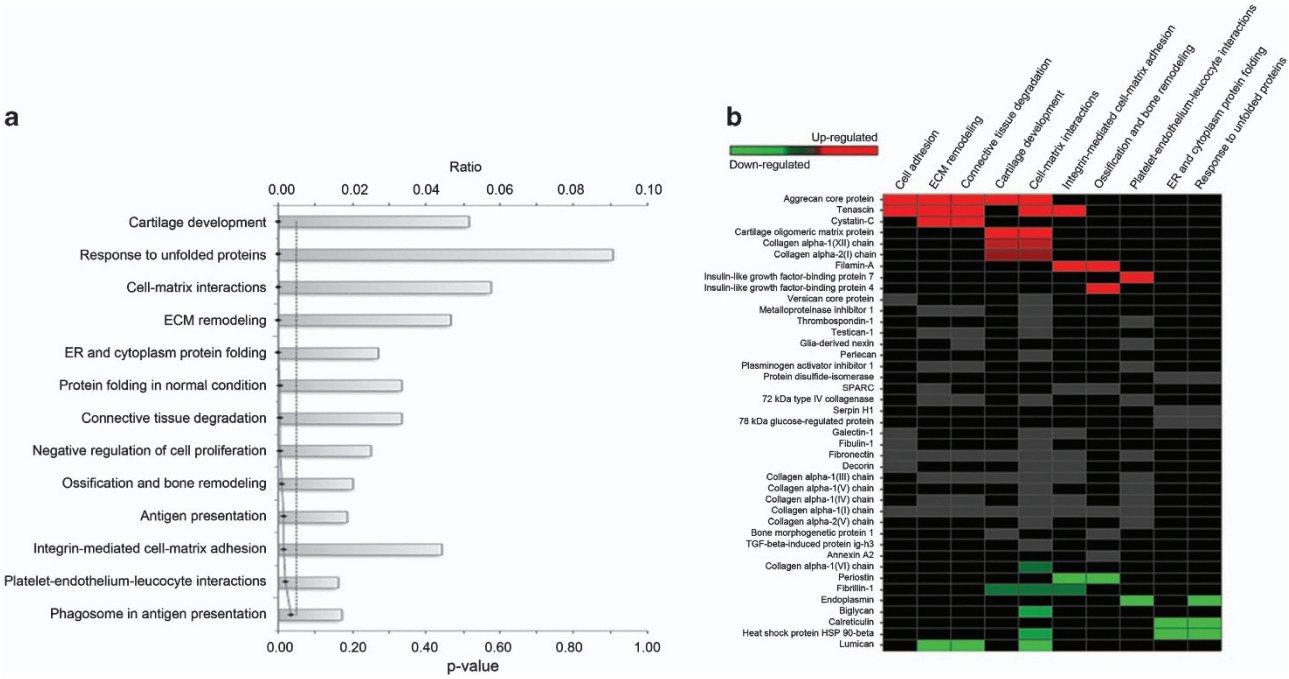

Figure 2 SASP of senescent MSC. (**a**) Enriched processes networks for differentially expressed proteins identified by LC-MS/MS analysis. The probability of a random intersection between the differentially expressed proteins with functional processes was evaluated by applying the hypergeometric test by using the Metacore software. (**b**) Heat map view representing the functional classification of up- and downregulated proteins in CM-P10 *versus* CM-P1. Significant functional terms were ranked according to enrichment scores generated using the annotation clustering algorithm in Metacore software

of the apoptosis level (Figure 3g and Supplementary Information, Supplementary Figure S2). Cellular senescence implicates a stable cell growth arrest. To evaluate the effects of IGFBP4/7 soluble factors on MSC growth capability, cell proliferation rate was evaluated on young MSC cultured with CM-P10 alone or treated with anti-IGFBP4 and/or anti-IGFBP7. CM-P10 treatment with anti-IGFBP4 or anti-IGFBP7 showed a significant increase of cell proliferation rates with respect to P1 MSC cultured with untreated CM-P10 at 72 h (Figure 3h). Interestingly, the simultaneous immunodepletion of both IGFBP4 and IGFBP7 resulted in a marked increase of cell proliferation starting from 24 h, thus supporting the view that blocking of IGFBP4/7 significantly dampens the pro-senescence activity of CM-P10.

The capability of IGFBP4 and IGFBP7 of triggering senescence phenomena in MSC was further confirmed by incubating young MSC with recombinant IGFBP4 and IGFBP7 (rIGFBP4/7). Indeed, the simultaneous addition of both rIGFBP4 and rIGFBP7 increased MSC senescence and induced apoptosis at the highest concentration assayed (Figures 3i and j).

Reversal of the DNA-damage response of young MSC induced by IGFBP4- and IGFBP7-immunodepleted CM-P10. Extensive investigations have revealed how the DNA damage-sensing and -signaling pathways, referred to as the DNA-damage response network, are linked to cellular senescence and apoptosis.[17,18] Therefore, the degree of DNA damage was investigated on young MSC cultured with IGFBP4- and IGFBP7-immunodepleted and non-immunodepleted CM-P10, by determining the level of phosphorylated histone H2A.X, which is considered a hallmark of damaged DNA nuclear foci.[17] A marked reduction of pH2A.X-positive cells was observed when P1 MSC were cultured with CM-P10 treated with both IGFBP4 and IGFBP7 antibodies (Figures 4a and b). Moreover, we determined the percentage of 8-oxo-deoxyguanosine (8-oxo-dG), a major product of oxidative damage to DNA.[19] In line with our results, the simultaneous blocking of IGFBP4 and IGFBP7 in CM-P10 significantly decreased the percentage of 8-oxo-dG-positive cells with damaged DNA (Figures 4c and d).

MSC senescence program affects ERK signaling. In response to different signals, multiple transduction pathways and targets are activated to induce cellular senescence responses. To determine the downstream pathway(s) triggered by the MSC 'senescence-messaging secretome' (SMS),[6] a network map including the differentially regulated proteins identified by MS analysis was constructed *in silico* by using the IPA software (Ingenuity Systems Inc., Redwood City, CA, USA) (Figure 5a). As shown, a specific subset of secreted proteins was mapped on a pathway converging, at intracellular level, on ERK 1/2. Previous evidences have demonstrated that the impairment of the nuclear/cytosolic localization of active ERK affects the senescence phenotype in human fibroblasts.[20,21] We therefore supposed that MSC senescence program may involve ERK signaling. To investigate this hypothesis, we analyzed the levels of total and activated ERK (pERK) in young and senescent MSC within different cellular compartments (Figure 5b). The relative distribution was computed as the ratio of the nuclear/cytoplasmic (N/C) ERK and pERK. Although the ratio N/C for

ERK was constant in P1 and P10, significant differences were detected with respect to pERK distribution. Indeed, the N/C ratio was strongly reduced only in P10 sample with a lower relative amount of nuclear *versus* cytoplasmic pERK in senescent MSC. Furthermore, together with an overall decrease of pERK levels following senescence induction,

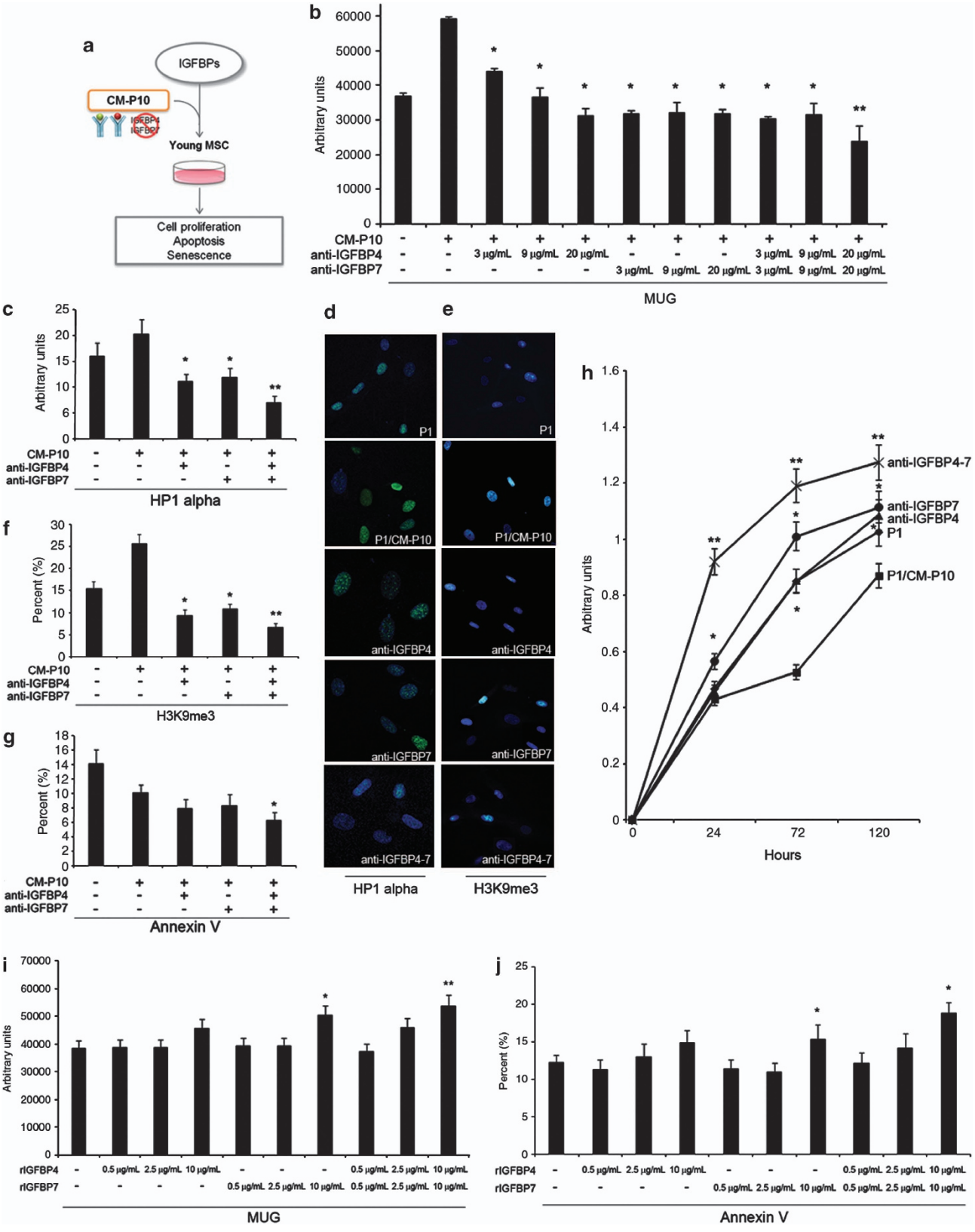

a fourfold decrease of nuclear pERK was revealed in P10 *versus* P1 MSC.

Discussion

Senescence is a physiological phenomenon leading to permanent cell growth arrest and impairment of cellular functions.[1,22] The extracellular microenvironment has a key role in regulating and determining the cellular response to senescence signaling. It is known that senescent cells secrete a unique repertoire of molecules (SASP) for which the term 'SMS' has been recently proposed.[6] Although the importance of changes in SMS has long been recognized, the molecular details of senescence signaling remain elusive. Furthermore, to the best of our knowledge, the senescence-induced extracellular response of stem cells has not been yet investigated. Given the peculiar properties of stem cells, including their multilineage differentiation capability, it is of fundamental importance to understand the response of stem cells to senescence signaling, also in view of their high potential in regenerative medicine and cancer therapy.

We demonstrate that MSC SASP implements a full senescence response in young cells, suggesting the presence, in the pool of secreted molecules, of factors capable of triggering, alone and/or in combination, senescence mechanisms through autocrine/paracrine signaling

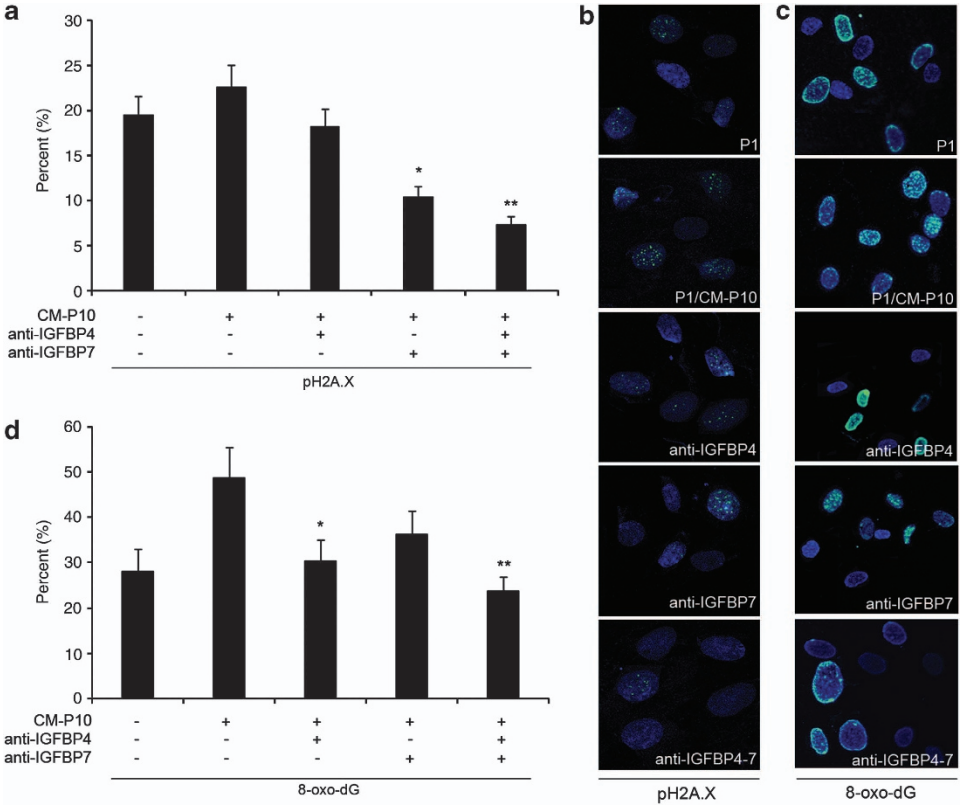

Figure 4 Reversal of the DNA-damage response of young MSC induced by CM-P10 by IGFBP4 and IGFBP7 blocking. (**a** and **b**) Phosphorylated H2A.X staining performed on young MSC cultured with untreated and IGFBP4 and/or IGFBP7 antibody-treated CM-P10; $*P<0.05$; $**P<0.01$ *versus* P1 MSC grown with untreated CM-P10. Fluorescence micrographs showing merge of representative fields of cells stained with anti-pH2A.X (green) and Hoechst 33342 (blue). (**c** and **d**) 8-oxo-dG staining performed on young MSC cultured with untreated and antibody-treated CM-P10. $*P<0.05$, $**P<0.01$ *versus* P1 MSC grown with untreated CM-P10. Fluorescence micrographs showing merge of representative fields of cells stained with anti-8-oxo-dG (green). Nuclei were counterstained with Hoechst 33342 (blue)

Figure 3 Secreted IGFBP4 and IGFBP7 induce senescence in young MSC. (**a**) Schematic summary of the experimental workflow for the investigation of the senescence-induction potential of IGFBP4 and IGFBP7. (**b**) MUG assay performed on young MSC cultured with untreated and antibody-treated CM-P10 at different concentrations (3, 9 and 20 μg/ml). Values are means of three independent experiments; $*P<0.05$; $**P<0.01$ *versus* P1 MSC grown with untreated CM-P10. (**c** and **d**) HP1 alpha detection performed on young MSC cultured with untreated and antibody-treated CM-P10. Micrographs showing merge of representative fields of P1 MSC grown under different conditions and stained with anti-HP1 alpha (green) to identify nuclear heterochromatin are showed. Nuclei were counterstained with Hoechst 33342 (blue); $*P<0.05$; $**P<0.01$ *versus* P1 MSC grown with untreated CM-P10. (**e** and **f**) H3K9me3 detection performed on young MSC cultured with untreated and antibody-treated CM-P10. Micrographs showing merge of representative fields of P1 MSC grown under different conditions and stained with anti-H3K9me3 (green) are showed. Nuclei were counterstained with Hoechst 33342 (blue); $*P<0.05$; $**P<0.01$ *versus* P1 MSC grown with untreated CM-P10. (**g**) Apoptosis assay of young MSC cultured with untreated and antibody-treated CM-P10; $*P<0.05$; *versus* P1 MSC grown with untreated CM-P10. (**h**) Cell proliferation assay on young MSC cultured with untreated and antibody-treated CM-P10. $*P<0.05$; $**P<0.01$ *versus* P1 MSC grown with untreated CM-P10. (**i** and **j**) MUG and Annexin V assays performed on young MSC cultured with rIGFBP4 and/or rIGFBP7 at different concentrations (0.5, 2.5 and 10 μg/ml). Values are means of three independent experiments; $*P<0.05$; $**P<0.01$ *versus* P1 MSC grown in control medium

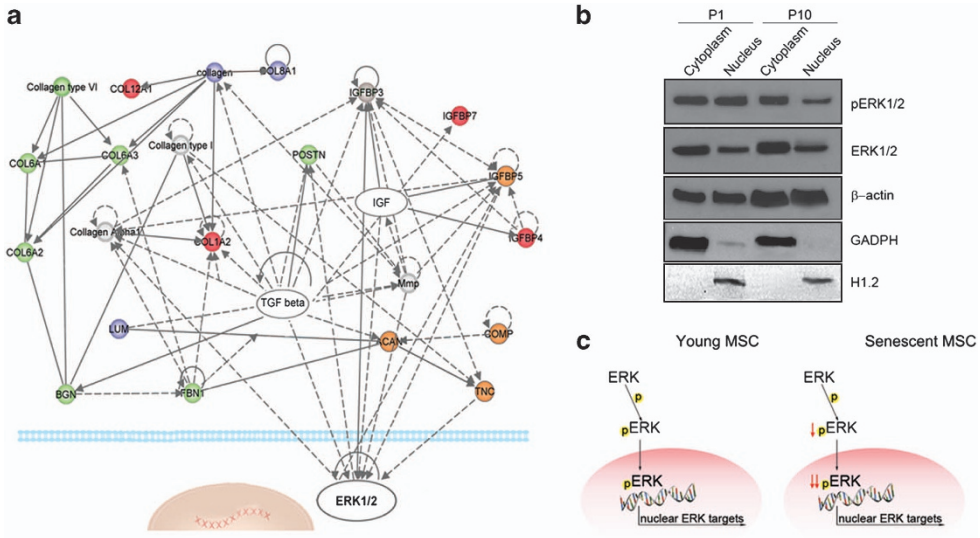

Figure 5 MSC senescence program involves the ERK 1/2 signaling. (**a**) Protein interaction network including a subset of differentially expressed proteins secreted by senescent MSC. The core molecules of the network were found to converge at extracellular level on IGF and TGF beta and, at intracellular level, on ERK 1/2 signaling pathways. According to IPA categorization, proteins uniquely detected or upregulated in senescent MSC are colored in orange and red, respectively; proteins uniquely detected or upregulated in young MSC are colored in blue and green, respectively. The pathway components identified by the algorithm or with no significant differences in their expression levels are reported in gray. Molecules are named according to IPA software as follows: COL12A1, Collagen alpha-1(XII); COL8A1, Collagen alpha-1(VIII); COL6A1, Collagen alpha-1(VI); COL6A3, Collagen alpha-3(VI); POSTN, Periostin; IGFBP, insulin-like growth factor binding protein; IGF, insuline-like growth factor; COL6A2, Collagen alpha-2(VI); COL1 A2, Collagen alpha-2(I); TGF beta, transforming growth factor beta; Mmp, Metalloproteinase protein family; COMP, Cartilage oligomeric matrix protein; TNC, Tenascin; ACAN, Aggrecan core protein; FBN1, Fibrillin-1; LUM, Lumican; BGN, Biglycan. (**b**) Western blot for ERK and pERK in N/C fractions of P1 and P10 MSC. To assess the purity of the N/C fractions, immunoblot analysis was performed with anti-GAPDH, as cytoplasmic marker, and anti-H1.2, as nuclear marker. Relative density of the bands was normalized to β-actin. (**c**) Schematic summary of the active ERK nucleo-cytoplasmic trafficking in the MSC response to replicative senescence induction

cascades. By performing a secretome-wide profiling of young and senescent MSC by LC-MS/MS, we have identified a subset of proteins characterizing their senescent phenotype, several of which involved in ECM remodeling and unfolded protein response. Consistent with our findings are previous studies reporting that ECM components can also influence their environment by mediating chemical and mechanical cues for tissue morphogenesis, proliferation and differentiation.[23] Upon cellular aging and senescence, an overall loss of junctional integrity, a thinning of the basement membrane and a progressive loss of ECM architecture are observed following a dysregulation in synthesizing the correct matrix components.[24,25] Our results show that besides the occurrence of significant changes in collagen composition, other ECM proteins (e.g., Fibrillin-1, Periostin, Lumican, Tenascin and Biglycan), involved in the maintaining of the structural and functional integrity of ECM, are differentially regulated in senescent cells. Furthermore, two components of the cartilage ECM matrix (i.e., Aggrecan and Cartilage oligomeric matrix protein, COMP) are specifically detected in senescent MSC. It has been reported that COMP interacts and is covalently cross-linked to the aggrecan core protein, and that the amount of these complexes increases with age.[26] In addition to ECM components, proteins associated to unfolded protein response are downregulated in senescent MSC. This finding is in agreement with the expected attenuation of molecular chaperone function and the resulting increase of protein misfolding and aggregation occurring during aging and senescence.[27] Among them, heat-shock protein 90-beta, downregulated in senescent MSC, is reported to be required for the correct assembly and function of telomerase complexes, which is an essential enzyme regulating cell life span.[28]

Key regulators of the IGF signaling pathways are differentially expressed in senescent *versus* young MSC. In particular, we detect several members of the IGFBP family (i.e., IGFBP2, IGFBP3, IGFBP4, IGFBP5 and IGFBP7). Although a role in senescence has been previously reported for IGFBP3 in human endothelial cells[29] and MCF-7 breast cancer cells,[30] we did not detect significant expression changes for this factor and his upstream regulator plasminogen activator inhibitor 1. This result, together with the simultaneous detection of other differentially expressed IGFBPs, suggests the activation of alternative senescence-inducing pathways in MSC. In particular, IGFBP5, previously reported to trigger senescence through a p-53 dependent mechanism,[31,32] is uniquely detected in senescent MSC.

The strong upregulation of two additional IGFBPs (i.e., IGFBP4 and IGFBP7) in senescent MSC prompted us to investigate their involvement in triggering MSC senescence and results provide new insights on the capability of IGFBP4 and IGFBP7 in promoting senescence in MSC. We indeed find that IGFBP4 and IGFBP7 are 'key players' in MSC SASP, because are involved in the induction of a senescent effect that strongly influences the functions of young cells. Blocking of IGFBP4 and/or IGFBP7 in CM-P10 reduces their pro-senescent effect on P1 MSC cultures. It is noteworthy that the simultaneous inhibition of IGFBP4 and IGFBP7 suppresses apoptosis and promotes cell growth, supporting their pleiotropic effect on MSC biology. Furthermore, the simultaneous

addition of rIGFBP4/7 increased senescence and induced apoptosis in MSC, and these effects were also observed with single addition of rIGFBP7. Our findings are in agreement with recent studies, demonstrating that IGFBPs have a causal role in the induction of senescence in cancer systems.[6] Reportedly, overexpression of IGFBP7 triggers BRAFV600E-induced senescence in human melanocytes[33,34] and is considered a tumor suppressor, as it reduces breast tumor growth by induction of senescence and apoptosis pathways.[35] Similarly, expression levels of IGFBP4 mRNA are increased in senescent hepatic stellate cells[36] and following induction of senescence-associated genes by 5-bromodeoxyuridine in HeLa cells.[37]

A critical aspect of senescence signaling is to unravel the connection between the SMS and the downstream effectors and pathways.[6] Recent evidences support the hypothesis that SMS-associated factors may be involved in distinct but integrated signaling pathways, and that the dynamic activation of intracellular cascades is responsible for the cell decision to eventually engage a senescence program.[6] However, the intracellular targets of SMS factors secreted by a given cell type have not been fully elucidated.[6] By using a bioinformatic approach, a specific subset of proteins of MSC SASP was mapped on a pathway converging on ERK 1/2. Wajapeyee *et al.*[33,38] demonstrated that IGFBP7 suppresses the phosphorylation of ERK and mediates its antiproliferative effects through a negative feedback signaling in oncogenic BRAFV600E-mediated senescence. In sharp contrast, previous evidences suggested that the expression of BRAFV600E induces the activation of ERK 1/2. These studies clearly demonstrate an involvement of the ERK signaling in the oncogene-induced senescence and point out the crucial role of ERK signaling in mediating different antiproliferative events such as apoptosis, autophagy and senescence.[20]

The plethora of signals that activate the ERK pathway and its numerous substrates suggest that the fine control of the spatiotemporal regulation of ERK activity is critical for determining opposite cell fates.[20] Activation of cytoplasmatic ERK 1/2 through its phosphorylation leads to nuclear translocation thus allowing the interaction with specific nuclear substrates and the induction of specific programs of gene expression. The regulation of ERK nucleo-cytoplasmic trafficking modulates the transfer efficiency of the signaling carried by activated ERK to the cell.[20] Accumulating evidences show that nuclear relocalization of active ERK is impaired in senescent human fibroblasts, and that this dysregulation may account for the irreversible proliferative arrest of senescent cells.[20] The impaired nuclear localization of active ERK and the loss of proliferative potential have been proposed to originate from either impaired nuclear import or from ERK inactivation. This interpretation is supported by the high activity of the nuclear ERK phosphatase MKP2/DUSP4 in senescent cells.[21]

Our results also attest a dysregulation of active ERK localization in stem cell senescence program, as a lower amount of nuclear *versus* cytoplasmic pERK is revealed in senescent MSC together with a decrease of nuclear pERK in P10 *versus* P1 MSC (Figure 5c). This finding strongly supports previous studies and further delineates an unexpected complexity of ERK signaling mechanisms in cellular senescence.[20] Indeed, we might envisage a scenario in which the nuclear/cytosolic localization of active ERK may be related to the MSC senescent phenotype as previously demonstrated for human fibroblasts.

Although more extensive studies are needed to expand our knowledge on the mechanisms underpinning the impaired ERK nucleo-cytoplasmic trafficking in stem cells, we also believe that our results pave the way to further investigations aiming to modify, in the near future, the current *in vitro* MSC expansion protocols for therapeutic purposes, thereby preventing or reducing the occurrence of negative senescence-related effects, and to better understand the complex process of senescence and aging in stem cells.

Materials and Methods

MSC cultures and preparation of CM. MSC were obtained and cultured as previously described.[39] Bone marrow was obtained from healthy donors after informed consent. Cells were separated on Ficoll density gradient (GE Healthcare, Milan, Italy) and the mononuclear cell fraction was collected and washed in PBS. Cells ($1–2.5 \times 10^5/cm^2$) were seeded in alpha-MEM containing 10% FBS and bFGF. After 72 h, non-adherent cells were discarded and adherent cells were further cultivated to confluency and amplified at P1. Replicative senescence was induced by repeatedly passaging the cells at P10. P1 and P10 cultures are referred to as 'young' and 'senescent' MSC, respectively. In our experimental conditions, it was verified that MSC cultures fulfilled the minimal criteria to define MSC.[40] All cell culture reagents were obtained by Euroclone Life Sciences (Milan, Italy) and Hyclone (Logan, UT, USA).

To harvest MSC secretome, 80% confluent P1 and P10 MSC cultures were extensively washed with PBS and transferred to a chemically defined, serum-free culture medium for an overnight incubation. Then, the CM from young (CM-P1) and senescent (CM-P10) MSC were collected and used at 50% in fresh alpha-MEM for *in vitro* cultivation of senescent and young MSC, respectively. Three independent culture preparations were prepared and pooled to address biological variation.

CM preparation for LC-MS/MS analysis. CM-P1 and CM-P10 were clarified by centrifugation, lyophilized and resuspended in 1 ml of 50 mM NH_4HCO_3. The proteins were then precipitated with 20% trichloroacetic acid for 30 min on ice and centrifuged for 15 min at $17\,500 \times g$.[41–43] Pellets washed with diethyl ether and acetone were air dried at room temperature, resuspended in 50 mM NH_4HCO_3, pooled and thoroughly sonicated into an ultrasonic bath for 10–15 min. Proteins were reduced with 2.5 mM dithiothreitol (final concentration) at 60 °C for 30 min and carbamidomethylated with 7.5 mM iodoacetamide (final concentration) at room temperature in the dark for 30 min. Enzymatic hydrolysis was performed by the addition of 10 μl of tosyl phenylalanyl chloromethyl ketone-treated trypsin solution (5 ng/μl) to the reduced and alkylated mixture. Digestion was performed by incubation at 37 °C for 16 h, followed by a second addition of 10 μl of trypsin incubated at 37 °C for 3 h. After digestion, samples were dried under vacuum in a SpeedVac Vacuum (Savant Instruments, Holbrook, NY, USA), resuspended in H_2O/CH_3CN/formic acid (FA) 95%/5%/0.1%, and peptides were purified by using macro spin columns (Harvard Apparatus, Holliston, MA, USA). Samples were dried, resuspended in 120 μl of 0.1% FA and centrifuged at $17\,500 \times g$ for 15 min. Aliquots of the supernatant (6 μl) were analyzed by ESI LTQ-OT MS.[41–43]

LC-MS configuration and protein identification. ESI LTQ-OT MS was performed on a LTQ Orbitrap Velos from Thermo Electron (San Jose, CA, USA) equipped with a NanoAcquity system from Waters (Waters Corporation, Manchester, UK).[43] Peptides were trapped on a home-made 5-μm 200 Å Magic C18 AQ (Michrom, Auburn, CA, USA) 0.1×20 mm pre-column and separated on a home-made 5-μm 100 Å Magic C18 AQ (Michrom) 0.75×150 mm column with a gravity-pulled emitter. The analytical separation was run for 65 min, using a gradient of H_2O/FA 99.9%/0.1% (solvent A) and CH_3CN/FA 99.9%/0.1% (solvent B), at a flow rate of 220 nl/min as follows: 5% solvent B for 1 min, from 5 to 35% solvent B in 54 min and from 35 to 80% solvent B in 10 min. For MS survey scans, the Orbitrap resolution was set to 60 000 and the ion population was set to 5×105 with an m/z window from 400 to 2000. Five precursor ions were selected for collision-induced dissociation in the LTQ by setting the ion population to 7×10^3 (isolation width of 2 m/z). The normalized collision energies were set to 35% for collision-induced dissociation.

Data processing was performed as previously described.[44,45] The Mascot software (Matrix Science, London, UK; version 2.2.0) was used for database searching against the Uniprot_sprot database release 2011_09 (21 September 2011, selected for *Homo sapiens*, 20 323 entries) assuming trypsin as digestion enzyme. Mascot was searched with a fragment ion mass tolerance of 0.60 Da and a parent ion tolerance of 25 p.p.m. Iodoacetamide derivative of cysteine was specified in Mascot as a fixed modification. Oxidation of methionine was specified in Mascot as a variable modification.

Scaffold software (version 4.0.1, Proteome Software Inc., Portland, OR, USA) was used to validate MS/MS-based peptide and protein identifications. Peptide identifications were accepted if they could be established at $>95\%$ probability.[46] Protein identifications were accepted if they could be established at $\geq 95\%$ probability and contained at least two identified unique peptides across replicate injection for each condition. Protein probabilities were assigned by the Protein–Prophet algorithm.[47] Proteins that contained similar peptides and could not be differentiated based on MS/MS analysis alone were grouped to satisfy the principles of parsimony. A false discovery rate value of 0.1% was calculated by using the Scaffold software for MS/MS validation.

Quantitative analysis. For protein quantification, for each identified protein, the number of spectral counts (the number of MS/MS spectra associated with an identified protein) was used to identify differentially expressed proteins.[48,49] To this end, normalized spectral counts were calculated by dividing the spectral counts for an identified protein by the sum of the spectral counts per sample. The statistical evaluation of proteins differentially expressed between the CM-P1 and CM-P10 samples was performed by applying the Fisher's exact test ($P<0.05$).

Bioinformatics analyses. Secreted and differentially expressed proteins identified in CM-P1 and CM-P10 were imported into the Ingenuity Pathways Analysis (IPA, Ingenuity Systems Inc.) or Metacore (GeneGo, St. Joseph, MI, USA) software for batch analysis and identification of the canonical pathways as previously reported.[41,43,50] An assessment of significantly enriched processes networks for differentially expressed proteins was performed by evaluating the probability of a random intersection between the differentially expressed proteins with functional processes by applying the hypergeometric test.[50] The heat map representing the functional classification of up- and downregulated proteins in CM-P10 *versus* CM-P1 was constructed by clustering significant functional terms according to the Metacore annotation algorithm by using the TIBCO Spotfire software (Somerville, MA, USA). Proteins with a predicted N-terminal signal sequence were identified by using SignalP 4.0,[51] available at http://www.cbs.dtu.dk/services/SignalP/ (set for eukaryotes using both neural networks and hidden Markov models), and were considered to be secreted via a classical pathway (endoplasmic reticulum/Golgi-dependent pathway). Identified proteins were also analyzed for secretion pathways according to SecretomeP 2.0 Server (http://www.cbs.dtu.dk/ services/SecretomeP/).[52] If the neural network exceeded or was equal to a value of 0.5 (NN-score ≥ 0.50), but no signal peptide was predicted, proteins were considered potentially secreted via a non-classical pathway.

Immunodepletion experiments. IGFBP4 and/or IGFBP7 were immunodepleted in CM-P10 by incubating CM and cells with a polyclonal anti-human IGFBP4 (Upstate Biotechnology, Lake Placid, NY, USA; catalog no. 06-109) and a polyclonal anti-human IGFBP7 (Santa Cruz Biotechnology, Dallas, TX, USA; catalog no. sc363293) at a final concentration of 3, 9 and 20 μg/ml for 30 min at 4 °C. Then, P1 MSC were cultured for 24 h at 37 °C with the CM-P10 treated with antibodies. After the incubation period, senescence was evaluated by MUG assay as described below. Cell proliferation and apoptosis were assessed by using CM-P10 immunodepleted with the highest antibody concentration (20 μg/ml).

Effect of recombinant IGFBP4 and IGFBP7 on MSC senescence and apoptosis. Recombinant human IGFBP4 and/or IGFBP7 (rIGFBP4 and rIGFBP7; PeproTech, London, UK; catalog nos. 350-05B and 350-09, respectively) were added to young MSC (P1) cultures at a final concentration of 0.5, 2.5 and 10 μg/ml. After a 36-h incubation period, senescence and apoptosis were evaluated by MUG and annexin V assays, respectively, as described below.

Cell proliferation and annexin V assays. Cell proliferation was evaluated by Quick Cell Proliferation Assay kit II (Biovision, Milpitas, CA, USA). One thousand cells were seeded in 96-well culture plates. At 1, 2 and 5 days post plating, cells were collected and counted. The ratio of the total number of cells at day 'n' to the number of cells at day 'n-1' was regarded as the cell proliferation rate.[53] Apoptotic cells were detected using fluorescein-conjugated annexin V (Roche, Milan, Italy) following the manufacturer's instructions.

Senescence assays. The percentage of senescent cells was calculated *in situ* by the number of blue β-galactosidase-positive cells out of at least 500 cells in different microscope fields as already reported.[54] For the quantitative SA-β-gal assay, 4-MUG was used as substrate of β-galactosidase. 4-MUG does not fluoresce until cleaved by the enzyme to generate the fluorophore 4-methylumbelliferone. Assay was carried out on lysates obtained from cells that were grown in 96-wells plates as reported.[55] The production of the fluorophore was monitored at an emission/excitation wavelength of 365/460 nm.

Cell fractionation. Cell fractionation was performed essentially as previously described.[56] P1 and P10 MSC were lysed in 10 mM Tris-HCl pH 7.4, 10 mM NaCl, 3 mM $MgCl_2$, 0.5 mM spermidine and 0.5% Nonidet P40. Following an incubation of 5 min at 4 °C, nuclear and cytosolic fractions were obtained after centrifugation for 5 min at 500 $\times$ *g*. The nuclei were washed three times in PBS, resuspended in the lysis buffer and further centrifuged at 17 500 $\times$ *g*.

Immunocytochemistry. Mouse monoclonal anti-8-oxo-dG (clone 2E2; Trevigen, Gaithersburg, MD, USA), rabbit monoclonal anti-phospho histone H2A.X (pH2A.X), rabbit polyclonal anti-HP1alpha (Cell Signaling, Danvers, MA, USA) and rabbit polyclonal anti-histone H3-trimethyl K9 (anti-H3K9me3, Abcam, Cambridge, UK) antibodies were used for the detection of 8-oxoguanine, pH2A.X, HP1 alpha and H3K9me3, respectively, according to the manufacturer's protocol. Nuclei were counterstained with Hoechst 33342 and cells were observed through a fluorescence microscope (Leica, Milan, Italy). The percentage of 8-oxo-dG-, HP1 alpha-, pH2A.X- and H3K9me3-positive cells was calculated by counting at least 500 cells in different microscope fields.

Western blot analysis. For western blot analysis, proteins from P1 and P10 MSC nuclear and cytosolic fractions (15 μg) were resolved by SDS-PAGE on a 4–15% Mini-Protean TGX precast gel (Bio-Rad, Milan, Italy) under reducing conditions and transferred onto nitrocellulose membrane (Bio-Rad) with a Trans-Blot Turbo electroblot apparatus (Bio-Rad). For the assessment of the purity of the nuclear and cytoplasmic fractions, monoclonal anti-GAPDH (1:20 000, Sigma, Milan, Italy; catalog no. G8795) and polyclonal anti-H1.2 (1:1000, Abcam; catalog no. ab17677) were used as cytoplasmic and nuclear markers, respectively. For the detection of ERK 1/2, anti-ERK 1 was used at a dilution of 1:2000 (Santa Cruz Biotechnology; catalog no. sc-93). Active (pERK) was detected by using an anti-phospho ERK 1/2 diluted 1:1000 (Cell Signaling; catalog no. 9101 L). Immunoreactive protein bands were visualized by the enhanced chemiluminescence (ECL) Plus Western Blotting Detection System (GE Healthcare) according to the manufacturer's instructions. Western blot results were normalized by stripping and reprobing the membranes with anti-β-actin monoclonal antibody (Sigma-Aldrich, Milan, Italy; catalog no. A2228) used for blot normalization. Densitometry analysis was performed with ImageJ software (http://rsb.info.nih.gov/ij/).

Conflict of Interest

The authors declare no conflict of interest.

Acknowledgements. This work was partially supported by Ministry of Foreign Affairs Republic of Italy (Senescence of stem cells and Rett syndrome), by European Energy Atomic Community FP-7-Fission 2012 RISK-IR) to UG and by Progetto PON - 'Ricerca e Competitivitá 2007–2013' - PON01_00802 entitled: 'Sviluppo di molecole capaci di modulare vie metaboliche intracellulari redox-sensibili per la prevenzione e la cura di patologie infettive, tumorali, neurodegenerative e loro delivery mediante piattaforme nano tecnologiche'.

1. Campisi J, d'Adda di Fagagna F. Cellular senescence: when bad things happen to good cells. *Nat Rev Mol Cell Biol* 2007; **8**: 729–740.
2. d'Adda di Fagagna F. Living on a break: cellular senescence as a DNA-damage response. *Nat Rev Cancer* 2008; **8**: 512–522.
3. Beyer Nardi N, da Silva Meirelles L. Mesenchymal stem cells: isolation, in vitro expansion and characterization. *Handb Exp Pharmacol* 2006; **174**: 249–282.
4. Pittenger MF, Mackay AM, Beck SC, Jaiswal RK, Douglas R, Mosca JD *et al*. Multineage potential of adult human mesenchimal stem cell. *Science* 1999; **284**: 143–147.

5. Valtieri M, Sorrentino A. The mesenchymal stromal cell contribution to homeostasis. *J Cell Physiol* 2008; **217**: 296–300.
6. Kuilman T, Peeper DS. Senescence-messaging secretome: SMS-ing cellular stress. *Nat Rev Cancer* 2009; **9**: 81–94.
7. Coppe JP, Patil CK, Rodier F, Sun Y, Munoz DP, Goldstein J *et al.* Senescence-associated secretory phenotypes reveal cell-nonautonomous functions of oncogenic RAS and the p53 tumor suppressor. *PLoS Biol* 2008; **6**: 2853–2868.
8. Fumagalli M, d'Adda di Fagagna F. SASPense and DDRama in cancer and ageing. *Nat Cell Biol* 2009; **11**: 921–923.
9. Caplan AI, Dennis JE. Mesenchymal stem cells as trophic mediators. *J Cell Biochem* 2006; **98**: 1076–1084.
10. Hsiao ST, Asgari A, Lokmic Z, Sinclair R, Dusting GJ, Lim SY *et al.* Comparative analysis of paracrine factor expression in human adult mesenchymal stem cells derived from bone marrow, adipose, and dermal tissue. *Stem cells Dev* 2012; **21**: 2189–2203.
11. Ranganath SH, Levy O, Inamdar MS, Karp JM. Harnessing the mesenchymal stem cell secretome for the treatment of cardiovascular disease. *Cell Stem Cell* 2012; **10**: 244–258.
12. van Koppen A, Joles JA, van Balkom BW, Lim SK, de Kleijn D, Giles RH *et al.* Human embryonic mesenchymal stem cell-derived conditioned medium rescues kidney function in rats with established chronic kidney disease. *PLoS One* 2012; **7**: e38746.
13. Pollina EA, Brunet A. Epigenetic regulation of aging stem cells. *Oncogene* 2011; **30**: 3105–3126.
14. Walter P, Gilmore R, Blobel G. Protein translocation across the endoplasmic reticulum. *Cell* 1984; **38**: 5–8.
15. Nickel W. The mystery of nonclassical protein secretion. A current view on cargo proteins and potential export routes. *Eur J Biochem* 2003; **270**: 2109–2119.
16. Narita M, Nunez S, Heard E, Narita M, Lin AW, Hearn SA *et al.* Rb-mediated heterochromatin formation and silencing of E2F target genes during cellular senescence. *Cell* 2003; **113**: 703–716.
17. Lombard DB, Chua KF, Mostoslavsky R, Franco S, Gostissa M, Alt FW. DNA repair, genome stability, and aging. *Cell* 2005; **120**: 497–512.
18. Roos WP, Kaina B. DNA damage-induced cell death by apoptosis. *Trends Mol Med* 2006; **12**: 440–450.
19. Alessio N, Squillaro T, Cipollaro M, Bagella L, Giordano A, Galderisi U. The BRG1 ATPase of chromatin remodeling complexes is involved in modulation of mesenchymal stem cell senescence through RB-P53 pathways. *Oncogene* 2013; **29**: 5452–5463.
20. Cagnol S, Chambard JC. ERK and cell death: mechanisms of ERK-induced cell death–apoptosis, autophagy and senescence. *Febs J* 2010; **277**: 2–21.
21. Tresini M, Lorenzini A, Torres C, Cristofalo VJ. Modulation of replicative senescence of diploid human cells by nuclear ERK signaling. *J Biol Chem* 2007; **282**: 4136–4151.
22. Rodier F, Campisi J. Four faces of cellular senescence. *J Cell Biol* 2011; **192**: 547–556.
23. Frantz C, Stewart KM, Weaver VM. The extracellular matrix at a glance. *J Cell Sci* 2010; **123**: 4195–4200.
24. Zhao CQ, Wang LM, Jiang LS, Dai LY. The cell biology of intervertebral disc aging and degeneration. *Ageing Res Rev* 2007; **6**: 247–261.
25. Yang KE, Kwon J, Rhim JH, Choi JS, Kim SI, Lee SH *et al.* Differential expression of extracellular matrix proteins in senescent and young human fibroblasts: a comparative proteomics and microarray study. *Mol Cells* 2011; **32**: 99–106.
26. Hauser N, Paulsson M, Heinegard D, Morgelin M. Interaction of cartilage matrix protein with aggrecan. Increased covalent cross-linking with tissue maturation. *J Biol Chem* 1996; **271**: 32247–32252.
27. Soti C, Csermely P. Molecular chaperones and the aging process. *Biogerontology* 2000; **1**: 225–233.
28. Holt SE, Aisner DL, Baur J, Tesmer VM, Dy M, Ouellette M *et al.* Functional requirement of p23 and Hsp90 in telomerase complexes. *Genes Dev* 1999; **13**: 817–826.
29. Kim KS, Kim MS, Seu YB, Chung HY, Kim JH, Kim JR. Regulation of replicative senescence by insulin-like growth factor-binding protein 3 in human umbilical vein endothelial cells. *Aging Cell* 2007; **6**: 535–545.
30. Elzi DJ, Lai Y, Song M, Hakala K, Weintraub ST, Shiio Y. Plasminogen activator inhibitor 1–insulin-like growth factor binding protein 3 cascade regulates stress-induced senescence. *Proc Natl Acad Sci USA* 2012; **109**: 12052–12057.
31. Kim KS, Seu YB, Baek SH, Kim MJ, Kim KJ, Kim JH *et al.* Induction of cellular senescence by insulin-like growth factor binding protein-5 through a p53-dependent mechanism. *Mol Biol Cell* 2007; **18**: 4543–4552.
32. Kojima H, Kunimoto H, Inoue T, Nakajima K. The STAT3-IGFBP5 axis is critical for IL-6/gp130-induced premature senescence in human fibroblasts. *Cell Cycle* 2012; **11**: 730–739.
33. Wajapeyee N, Serra RW, Zhu X, Mahalingam M, Green MR. Oncogenic BRAF induces senescence and apoptosis through pathways mediated by the secreted protein IGFBP7. *Cell* 2008; **132**: 363–374.
34. Wajapeyee N, Serra RW, Zhu X, Mahalingam M, Green MR. Role for IGFBP7 in senescence induction by BRAF. *Cell* 2010; **141**: 746–747.
35. Benatar T, Yang W, Amemiya Y, Evdokimova V, Kahn H, Holloway C *et al.* IGFBP7 reduces breast tumor growth by induction of senescence and apoptosis pathways. *Breast Cancer Res Treat* 2012; **133**: 563–573.
36. Schnabl B, Purbeck CA, Choi YH, Hagedorn CH, Brenner D. Replicative senescence of activated human hepatic stellate cells is accompanied by a pronounced inflammatory but less fibrogenic phenotype. *Hepatology* 2003; **37**: 653–664.
37. Suzuki T, Minagawa S, Michishita E, Ogino H, Fujii M, Mitsui Y *et al.* Induction of senescence-associated genes by 5-bromodeoxyuridine in HeLa cells. *Exp Gerontol* 2001; **36**: 465–474.
38. Denoyelle C, Abou-Rjaily G, Bezrookove V, Verhaegen M, Johnson TM, Fullen DR *et al.* Anti-oncogenic role of the endoplasmic reticulum differentially activated by mutations in the MAPK pathway. *Nat Cell Biol* 2006; **8**: 1053–1063.
39. Alessio N, Bohn W, Rauchberger V, Rizzolio F, Cipollaro M, Rosemann M *et al.* Silencing of RB1 but not of RB2/P130 induces cellular senescence and impairs the differentiation potential of human mesenchymal stem cells. *Cell Mol Life Sci* 2013; **70**: 1637–1651.
40. Dominici M, Le Blanc K, Mueller I, Slaper-Cortenbach I, Marini F, Krause D *et al.* Minimal criteria for defining multipotent mesenchymal stromal cells. The International Society for Cellular Therapy position statement. *Cytotherapy* 2006; **8**: 315–317.
41. Farina A, D'Aniello C, Severino V, Hochstrasser DF, Parente A, Minchiotti G *et al.* Temporal proteomic profiling of embryonic stem cell secretome during cardiac and neural differentiation. *Proteomics* 2011; **11**: 3972–3982.
42. Severino V, Farina A, Colucci-D'Amato L, Reccia MG, Volpicelli F, Parente A *et al.* Secretome profiling of differentiated neural mes-c-myc A1 cell line endowed with stem cell properties. *Biochim Biophys Acta* 2013; **1834**: 2385–2395.
43. Severino V, Farina A, Chambery A. Analysis of secreted proteins. *Methods Mol Biol* 2013; **1002**: 37–60.
44. Scherl A, Tsai YS, Shaffer SA, Goodlett DR. Increasing information from shotgun proteomic data by accounting for misassigned precursor ion masses. *Proteomics* 2008; **8**: 2791–2797.
45. Mueller LN, Rinner O, Schmidt A, Letarte S, Bodenmiller B, Brusniak MY *et al.* SuperHirn - a novel tool for high resolution LC-MS-based peptide/protein profiling. *Proteomics* 2007; **7**: 3470–3480.
46. Keller A, Nesvizhskii AI, Kolker E, Aebersold R. Empirical statistical model to estimate the accuracy of peptide identifications made by MS/MS and database search. *Anal Chem* 2002; **74**: 5383–5392.
47. Nesvizhskii AI, Keller A, Kolker E, Aebersold R. A statistical model for identifying proteins by tandem mass spectrometry. *Anal Chem* 2003; **75**: 4646–4658.
48. Kulasingam V, Diamandis EP. Proteomics analysis of conditioned media from three breast cancer cell lines: a mine for biomarkers and therapeutic targets. *Mol Cell Proteomics* 2007; **6**: 1997–2011.
49. Wilson R, Diseberg AF, Gordon L, Zivkovic S, Tatarczuch L, Mackie EJ *et al.* Comprehensive profiling of cartilage extracellular matrix formation and maturation using sequential extraction and label-free quantitative proteomics. *Mol Cell Proteomics* 2010; **9**: 1296–1313.
50. Rocco M, Malorni L, Cozzolino R, Palmieri G, Rozzo C, Manca A *et al.* Proteomic profiling of human melanoma metastatic cell line secretomes. *J Proteome Res* 2011; **10**: 4703–4714.
51. Bendtsen JD, Nielsen H, von Heijne G, Brunak S. Improved prediction of signal peptides: SignalP 3.0. *J Mol Biol* 2004; **340**: 783–795.
52. Bendtsen JD, Jensen LJ, Blom N, Von Heijne G, Brunak S. Feature-based prediction of non-classical and leaderless protein secretion. *Protein Eng Des Sel* 2004; **17**: 349–356.
53. Nakamura S, Yamada Y, Baba S, Kato H, Kogami H, Takao M *et al.* Culture medium study of human mesenchymal stem cells for practical use of tissue engineering and regenerative medicine. *Biomed Mater Eng* 2008; **18**: 129–136.
54. Debacq-Chainiaux F, Erusalimsky JD, Campisi J, Toussaint O. Protocols to detect senescence-associated beta-galactosidase (SA-betagal) activity, a biomarker of senescent cells in culture and *in vivo*. *Nat Protoc* 2009; **4**: 1798–1806.
55. Gary RK, Kindell SM. Quantitative assay of senescence-associated beta-galactosidase activity in mammalian cell extracts. *Anal Biochem* 2005; **343**: 329–334.
56. Liu H, Kang H, Liu R, Chen X, Zhao K. Maximal induction of a subset of interferon target genes requires the chromatin-remodeling activity of the BAF complex. *Mol Cell Biol* 2002; **22**: 6471–6479.

Supplementary Information accompanies this paper on Cell Death and Disease website (http://www.nature.com/cddis)